Confocal Raman Microspectroscopy and Imaging Study of Theraphthal in Living Cancer Cells

Alexei V. Feofanov,[*] Alexei I. Grichine,[*] Larissa A. Shitova,[†] Tatyana A. Karmakova,[†] Raisa I. Yakubovskaya,[†] Marguerite Egret-Charlier,[‡] and Paul Vigny[‡]

[*]Shemyakin-Ovchinnikov Institute of Bioorganic Chemistry, Russian Academy of Sciences, 17871 Moscow, Russia; [†]Hertsen Moscow Oncological Institute, 125284 Moscow, Russia; and [‡]Center de Biophysique Moleculaire, CNRS UPR 4301, University of Orleans, 45071 Orleans, France

ABSTRACT Binary systems combining a transition metal complex and ascorbate have been proposed recently for catalytic therapy of malignant tumors. The killing effect on tumor cells is achieved by production of free radicals in the course of accelerated oxidation of ascorbate by dioxygen in the presence of transition metal complexes. Further progress in the development of binary catalytic systems (BCSs) requires a special method for their investigation in cells and tissues, because neither component of BCSs fluoresces. Here a resonance Raman confocal spectral imaging (RR CSI) technique was introduced as a unique approach to monitor quantitatively the transition metal complexes within living cells. Intracellular accumulation, localization, and retention of theraphthal (TP), a catalyst of the advanced TP/ascorbate BCS, were investigated in A549 cells with the RR CSI technique. The cellular analysis was complemented with the detailed study of molecular interactions of TP in solution and environmental factors affecting the RR spectrum of TP. TP does not penetrate into membranes, it binds very weakly to DNA and RNA, but it readily forms complexes with proteins. Binding with Ca^{2+} cations and decreasing pH below 6 induce aggregation of TP. By analyzing RR spectra recorded from every point within a TP-treated cell, three states of the agent were discriminated, namely, monomeric TP in polar environment, TP bound to proteins, and aggregated TP. Their cytoplasmic and nuclear distributions were mapped at different stages of uptake and efflux. By introducing organelle-selective fluorescent probes into drug-treated cells and measuring intracellular localization of both the probe and the drug, compartmentation of TP was revealed. Cell growth suppression by the TP/ascorbate system was measured, and probable molecular and organelle targets of radical damage were characterized.

INTRODUCTION

The continuous search for new approaches to the effective treatment of cancer diseases recently resulted in the development of binary catalytic systems (BCSs) (Kimoto et al., 1983; Vol'pin et al., 1996, 1998; Belkov et al., 1996; Bubnovskaya et al., 1998). Similar to x-ray therapy and photodynamic therapy, an antitumor action of these systems is related to the production of free radicals, which induce oxidative degradation of molecules and organelles of cancer cells. BCSs employ a transition-metal complex as a catalyst and a second molecule as a substrate. Autooxidation of the substrate produces reactive oxygen species. The catalyst accelerates this process strongly. Selective accumulation of BCS components within malignant cells and/or in tumor tissue is a necessary prerequisite for intense radical attack followed by tumor growth suppression and necrosis.

The first attempt at BCS development for anticancer applications was reported by Kimoto et al. (1983). A killing effect on tumor cells and an increase in the life span of mice after inoculation of tumor cells were achieved with copper: glycylglycylhistidine complex and ascorbate as a substrate. Recently, several promising new BCSs were discovered. It was found that a combination of cobalt or iron phthalocyanine and sodium ascorbate has high in vitro and in vivo antitumor activity (Vol'pin et al., 1996; Belkov et al., 1996). These BCSs have been patented as new agents for binary catalytic therapy of malignant tumors (Vol'pin et al., 1995). A combination of theraphthal (TP, cobalt (II) octa-4,5-carboxyphthalocyanine) (Fig. 1) and ascorbate was approved for phase I of a clinical trial. Pronounced cytotoxic activity was found also for BCSs by employing complexes of Co with vitamin B_{12} and its derivatives (Vol'pin et al., 1998) and complexes of Co with tetradentate Schiff bases having an MN_2O_2 coordination center, where M is metal (Bubnovskaya et al., 1998).

Ascorbate is currently considered the most suitable substrate for BCS. It is known that some human tumors accumulate ascorbate to a greater extent than do normal tissues (Honegger et al.,1988). Ascorbate is easily oxidized by oxygen in the presence of transition metal ions and produces reactive oxygen species such as H_2O_2, $O_2^{-\bullet}$, and OH^- (Halliwell and Foyer, 1976). Moreover, some products of ascorbate oxidation have considerable antitumor effects themselves (Cameron et al., 1979; Pierson et al., 1985; Poydock, 1991).

During the last few years there has been a gradual increase in the knowledge of in vitro and in vivo antitumor effects induced by various BCSs under different regimes of treatment (Vol'pin et al., 1996, 1998; Syrkin et al., 1998; Bubnovskaya et al., 1998). Biodistribution and retention of

Received for publication 29 July 1999 and in final form 28 September 1999.

Address reprint requests to Dr. Alexei Feofanov, Shemyakin-Ovchinnikov Institute of Bioorganic Chemistry, Russian Academy of Sciences, ul. Miklukho-Maklaya 16/10, 117871, Moscow, Russia. Tel.: 7095–3366455; Fax: 7095–3361766; E-mail: alexei@nmr.ru.

0006-3495/00/01/499/14 $2.00

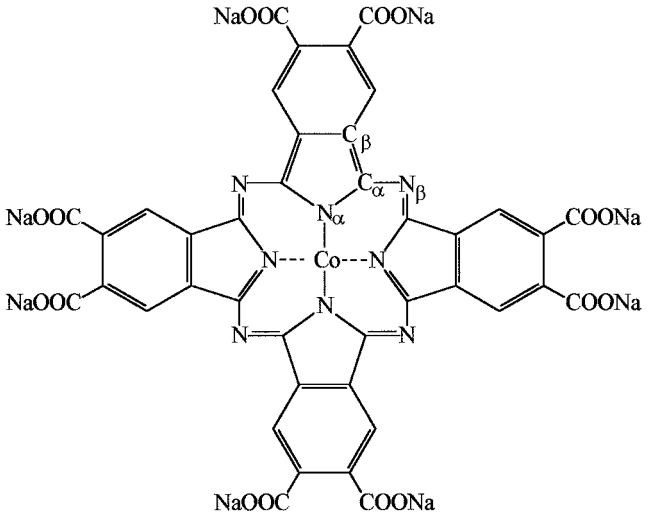

FIGURE 1 Structure of theraphthal (TP).

some catalysts employed in BCSs were characterized in organs and tissues by the use of extractive and fractionative analytical techniques. However, practically nothing is known about the localization and distribution of transition metal complexes in cells and tissue structures at the microscopic level. The problem is that paramagnetic metals such as Cu, Co, and Fe shorten the lifetime of the excited state of the complex, making the dye nonfluorescent and nonphotoactive. As a result, nondestructive detection and in situ investigation of transition metal complexes in living cells and tissues are much more complicated compared to those of fluorescent drugs.

Further progress in directed synthesis and the study of new compounds with improved catalytic and pharmacological characteristics requires comprehensive understanding of the behavior of BCS components in living systems, revealing the correlation between the chemical structure of the catalyst and its localization within cells, and the proximity of the drug to the critical targets of its action. The first attempt to apply the confocal direct Raman imaging method to investigation of the localization of some transition metal complexes (including TP) within cells was reported elsewhere (Arzhantsev et al., 1999). The present work is aimed at introducing the resonance Raman (RR) confocal spectral imaging (CSI) technique for the detection and study of nonfluorescent transition-metal complexes in living cells.

The CSI technique is an advanced approach to quantitative monitoring of anticancer drug localization within living cells with three-dimensional (3D) micron resolution. The method is based on recording in confocal mode and analysis of the whole spectrum of the drug from each point inside the cell. It provides an important advantage in comparison with other imaging methods that measure integrated signal intensity selected by either broad- or narrowband filters; with the CSI technique all of the spectrum parameters are accessible to analysis. Thus the CSI technique allows the main principles of spectral analysis, which are widely used to study molecular interactions in solution, to be transferred to the cellular level. It provides a unique opportunity to identify and to map intracellular molecular interactions of drugs. It opens the way to the study and direct comparison of molecular interactions in solution and within living cells.

According to the CSI technique the creation of spectral images is based on a decomposition procedure that is applied to a set of spectra measured from within the cell. Each original spectrum is decomposed into a sum of reference spectra with appropriate coefficients. The reference spectra are attributed to different states and specific interactions of the drug within cells. The reference spectra originate from a set of characteristic spectra corresponding to possible molecular interactions and environmental effects observed for the drug in solution. Two-dimensional (2D) maps of decomposition coefficients (spectral images) describe subcellular distribution of the drug and its complexes.

The CSI technique was initially developed for the investigation of fluorescent drugs (Sharonov et al., 1994a; Feofanov et al., 1997a,b). In the present work its applicability to the study of nonfluorescent drugs in living cells is demonstrated for the first time. The molecule has to absorb in a visible region to be detectable in cells with RR spectroscopy. Although the resonance Raman CSI technique does not provide sensitivity comparable to that of fluorescence microscopy, it is the only approach allowing molecular interactions and distribution of nonfluorescent drug to be studied with 3D micron resolution in living cells.

The high informational content of Raman and RR spectroscopy has been duly demonstrated in investigations of biological molecules and their supramolecular complexes, as well as in a variety of biological and medical applications (Clark and Hester, 1993). RR microspectroscopic studies of chromophore-containing biological molecules in living cells have been reviewed recently (Greve and Puppels, 1993; Puppels and Greve, 1996). Point measurements performed in these cellular investigations were aimed at characterizing structure and/or functional states of studied molecules in particular cellular organelles or domains. To measure the localization and continuous distribution of Raman scattering species along microspecimens, several approaches to micro-Raman image recording have been realized on a basis of narrow-band interference filtering (Puppels et al., 1993; Williams et al., 1994), tunable acoustooptic filtering (Treado et al., 1992), Hadamard multiplexing (Treado and Morris, 1990; Liu et al., 1991), and confocal scanning (Sharonov et al., 1994b; Sijtsema et al., 1998) techniques. The first three approaches are wide-field or global imaging methods that allow the acquisition of Raman data on a time-consuming point-by-point (or line-by-line) basis to be avoided, but at the expense of the absence of axial resolution. The filtering methods employ a 2D camera to record

Raman scattering from the specimen area illuminated by a defocused laser beam. The spectral range to be detected is selected in this case with the filter, and it can be as narrow as 20 cm^{-1} (Greve and Puppels, 1993; Puppels and Greve, 1996). The filtering method can also be realized on the basis of the point-by-point (or line-by-line) confocal scanning of the sample with the focused laser beam to provide the 3D resolution (Sijtsema et al., 1998). The filtering techniques are the most useful in the applications where 2D mapping of a specimen can be made using the a priori known spectral markers. In a more general case an extensive preliminary Raman microspectroscopy examination of the sample is required to identify spectral bands that are best suited for recording the Raman images. Just a few applications of Raman imaging techniques to the study of living cells have been published up to date (Greve and Puppels, 1993; Sijtsema et al., 1998; Arzhantsev et al., 1999). They have been concerned with the intracellular distribution of chromophore-containing molecules.

In the present work the CSI approach was realized on the basis of RR spectroscopy for the investigation of TP within living cells. The combination of TP with ascorbate is one of the most advanced BCSs (Syrkin et al., 1998). As a necessary step to a deep understanding of mechanisms of cell killing and critical cellular targets, the molecular interactions of TP and its intracellular accumulation, localization, and retention were investigated. Compartmentation of TP was studied by introducing organelle-selective fluorescent probes into drug-treated cells and measuring the intracellular distribution of both the probe and the drug. Cell growth suppression with this BCS was also measured. The influence of radical attack on the cellular organelles was examined by the use of selective fluorescent probes.

MATERIALS AND METHODS

Chemicals

TP was received from NIOPIK (Moscow, Russia). A stock solution of TP (1 mM) was prepared in phosphate-buffered saline (PBS) for cellular experiments and in 20 mM Tris-HCl buffer (pH 7.4) for measurements in solution. The concentration of TP in aqueous buffer solution was measured by absorption, using an extinction coefficient $\epsilon_{675} = 1 \times 10^5\ M^{-1}\ cm^{-1}$.

Calf thymus DNA, calf liver RNA, human and bovine serum albumins, chicken egg white lysozyme, ethidium bromide (EtBr), and 3-[4,5-dimethylthiazol-2-yl]-2,5-diphenyltetrazolium bromide (MTT) were purchased from Sigma (St. Louis, MO). Gentamicine, L-glutamine, fetal calf serum, and minimum essential medium (MEM)-Eagle culture medium were purchased from MGIEM (Russia). Acridine orange (AO), rhodamine 123 (Rh123), and sodium ascorbate were purchased from ICN (Costa Mesa, CA). All other chemicals used in this work were of analytical-reagent grade.

An extract of nonhistone proteins from cell nuclei was a gift of Dr. L. G. Nikolaev. The extraction was performed following a slightly modified procedure described elsewhere (Dignam et al., 1983). Histone H2A was a gift of Dr. V. L. Karpov.

Sample preparation for experiments in solution

Mixtures of TP with human (140 μM) and bovine (140 μM) serum albumins, lysozyme (600 μM), nonhistone proteins (10 mg/ml), histone H2A (100 μM), RNA (1.6 mM), and DNA (1.7 mM bp) were prepared in buffer solution (20 mM Tris-HCl, pH 7.4). Detergent-containing solutions of TP were prepared at the critical micelle concentration of Triton X-100 (*t*-octylphenoxypolyethoxyethanol, 0.24 mM) or sodium dodecyl sulfate (8.27 mM) in buffer solution (20 mM Tris-HCl, pH 7.4). The solutions were prepared at 2 and 50 μM concentrations of TP for spectrophotometric and microspectroscopic measurements, respectively.

Cells

A549 human lung adenocarcinoma cells were obtained from the Ivanovsky Institute of Virology, Russian Academy of Medical Sciences. Cells were cultured in 25 cm^2 culture flasks at 37°C, 5% CO_2 in MEM-Eagle culture medium supplemented with 10% fetal calf serum inactivated with heating and 0.03% L-glutamine. Cells were removed from flask walls with 25 mM EDTA.

Cell treatment

For survival assays cells were seeded in 96-well plates (Costar) at 5×10^4 cells/ml and incubated for 24 h in culture medium. Stock solutions of TP (1 mM) and sodium ascorbate (300 mM) were prepared in PBS. TP was added gradually into wells to achieve final concentrations from 3 to 100 μM in approximately twofold increments. Ascorbate was introduced 15 min later at a TP/ascorbate molar ratio of 1:20. Cells were incubated with reagents for 48 h in a CO_2 incubator, then inhibition of cell growth was determined with an MTT test according to the procedure described elsewhere (Carmichael et al., 1987).

For microscopic experiments cells were grown on coverglasses in wells of 24-well plates (Costar) for 24 h. The sowing density was 5×10^4 cells/ml. To study drug uptake, cells were incubated with 100 or 400 μM of TP for 10 min or 1, 3, 6, or 14 h. To investigate drug efflux the cells were treated with 400 μM TP for 6 h, rinsed twice with warm (37°C) PBS solution (pH 7.4), and incubated in TP-free culture medium for 2 or 9 h. When cells were treated with TP/ascorbate mixture, sodium ascorbate (8 mM) was added to the medium 15 min after TP (400 μM) was introduced. Cells were incubated with the TP/ascorbate mixture for 3 or 6 h.

Selective labeling of cellular organelles was performed as follows. Cells incubated with 100 μM TP, TP/ascorbate mixture (100 μM/2 mM), or 2 mM sodium ascorbate for 1 h or 3 h were rinsed twice with warm PBS solution and treated for 10 min with 10 μg/ml AO, 5 μg/ml EtBr mixture, or 10 μg/ml Rh123. Then cells were rinsed twice with PBS solution. To identify sites of TP localization, cells were incubated with 400 μM TP for 2 h before staining with vital dyes.

For microscopic observations and measurements a glass with cells was placed on a microscope slide and covered with a coverglass. To prevent cells from drying during measurements, PBS solution (60 μl) was introduced under the coverglass.

Spectral measurements

Absorption spectra were measured with a Cary-209 spectrophotometer (Varian, Sunnyvale, CA). To estimate an extent (α) of TP binding with nucleic acids and proteins, the spectral decomposition of the absorption spectrum of the TP/ligand mixture into the spectrum of the free drug and another part, corresponding to a bound drug, was performed. The value of α was calculated as follows:

$$\alpha = (1 - C_f/C_0) \times 100\% \quad (1)$$

where C_0 and C_f are, respectively, the total concentration of the drug and the concentration of free drug in the TP/ligand mixture.

CSI measurements were performed using a V-45 installation (Dilor, Lille, France) for scanning confocal microspectroscopy and imaging (Favard et al., 1999). The Optiphot-2 microscope (Nikon, Japan) integrated into this device was equipped with an epifluorescence unit. A sliding mirror provided a choice between different regimes of specimen study: observation of a cell in transmitted white light, or epifluorescent measurements, or CSI measurements. The latter option was used in the present study to make a microphotograph of the cell, to record a confocal spectral image of TP distribution, and to observe the distribution of the selective label of cellular organelles with the epifluorescence unit in the same cell. Lateral and axial resolution in CSI measurements was ~1 and ~4 μm, respectively, when a 100× oil immersion objective was used. Spectral resolution was 5 cm^{-1}. A motorized sample stage was used to provide a point-by-point scanning regime. The 30 × 30 or 40 × 40 point spectral images were recorded with 632.8-nm excitation wavelength of a He-Ne laser (0.3 mW). The recording time for a 40 × 40 point spectral image was 15–20 min.

The procedures of spectrum treatment and spectral image creation were described earlier (Sharonov et al., 1994a,b; Feofanov et al., 1995). Briefly, each experimental spectrum recorded in confocal mode from within cells was decomposed as a sum of reference spectra with appropriate coefficients. The reference spectra were carefully selected, based on the results of model experiments in solution, to describe adequately different states of the drug inside a cell (in this case monomers, aggregates, and complexes of TP with proteins). The integrated intensity of each reference spectrum multiplied by the decomposition coefficient for each point produced a 2D map (hereafter referred to as the spectral image) that characterized the relative distribution of monomers (aggregates, complexes with proteins) of TP within the cell.

The calibration procedures have been performed to estimate subcellular concentration of monomeric theraphthal (TP_{mono}) and theraphthal bound to proteins (TP_{bnd}), based on the integral intensity of the corresponding micro-Raman spectra. The spectra of TP and TP bound to proteins were measured in aqueous buffer solution with a microscope under the experimental conditions (optical pathway, geometry of light collection, lateral and axial resolution, laser power, integration time) used for recording the confocal spectral images. The calibration curves showed the linear dependence of RR signal intensity on TP concentration. An inner filter effect caused very little deviation from linearity, inasmuch as exciting and scattered light passed the absorbing layer of 10–20 μm only.

To quantify intracellular TP, a 2D set of the spectra measured from a cell was decomposed into components corresponding to the set of reference spectra, and RR intensities of the components corresponding to TP_{mono} and TP_{bnd} were recalculated into concentrations based on results of the calibration procedure. The amount of aggregated drug cannot be described in terms of concentration. However, Raman intensity is proportional to the amount of aggregates in each microvolume. Thus the relative quantity of aggregates in different cellular compartments was compared based on the intensity of the RR signal of the aggregated TP (TP_{agg}) component. Such a comparison was also performed for neighboring cells and for cells incubated with the drug at different regimes. This was done while 1) carefully maintaining the alignment of installation and keeping the experimental conditions of measurements unchanged, 2) periodically checking the intensity of the RR signal of reference TP solution in the course of series of experiments.

All of the measurements have been repeated in two independent experiments. Intracellular concentrations of TP were averaged over 20 cells for each measurement. Standard deviations were 0.5–0.7 of average values. These deviations were related to differences in the drug uptake by particular cells and were much more than errors of measurements and calculations (10–15%).

To measure RR cross sections of TP vibrational modes, the sample was dissolved in a buffer (20 mM Tris-HCl, pH 7.4) that contained high-purity sodium sulfate (0.5 M) as an internal standard of Raman intensity. RR cross sections of TP vibrational modes were calculated according to the equation

$$\sigma_n = \sigma_s I_n C_s I_s^{-1} C_n^{-1} \quad (2)$$

where the subscript index n shows that the parameter corresponds to the vibrational mode of TP and s to the 981 cm^{-1} band of the internal standard, and σ_n is the RR cross section for vibrational mode n at the 632.8-nm excitation wavelength. I is the integral intensity of the Raman band. C_s and C_n are the molar concentrations of sodium sulfate and TP, respectively. The Raman cross section (σ_s) of the 981 cm^{-1} sulfate vibrational mode at 632.8 nm excitation was calculated using the parameters estimated elsewhere (Fodor et al., 1989) and found to be 1.6×10^{-30} cm^2 sr^{-1} $molecule^{-1}$.

RR cross sections of vibrational modes of TP bound to protein were calculated based on the known RR cross sections for free TP and taking into account differences in intensity of the RR spectra of equimolar solutions of TP in buffer solution and TP/protein complex that were recorded under the same experimental conditions. It should be mentioned that it was not possible to use sodium sulfate as an internal standard of Raman intensity to measure RR cross sections of TP bound to protein, because the high ionic strength of the solution affects considerably the interactions of the drug with proteins.

RESULTS

Molecular interactions and environmental factors affecting TP state in solution

Investigation of molecular interactions of TP in solution is a necessary prerequisite for analysis of the drug in a cellular environment. It helps one to understand the ability of TP to bind to different cellular molecules and structures, thus revealing probable intracellular complexes of the drug. The knowledge of characteristic spectral changes induced by environmental factors (pH, hydrophobicity, ionic composition, drug concentration, etc.) assists the analysis of the TP microenvironment within cells.

Raman spectra of TP were excited with a wavelength of 632.8 nm, which is in preresonance with the Q absorption band (675 nm). RR spectra of TP were recorded in the 800-1800 cm^{-1} range because the lower frequency region was obscured by a strong Raleigh scattering in the cellular microspectroscopic studies. The RR spectrum of TP (Fig. 2) contains bands related to vibrational modes of phthalocyanine chromophore (Table 1). The Q band is largely due to vibronic transitions associated with the inner macrocycle and the five-membered rings, whereas the six-membered rings are involved only weakly (Bartholomew et al., 1989). Accordingly, vibrational modes of the molecular moieties related to Q-band transitions are enhanced in the RR spectrum. Carboxyl groups are very weakly conjugated with the π-electron system of phthalocyanine. Thus vibrations of carboxyl groups are not enhanced and do not contribute to the RR spectrum of TP. The phthalocyanine vibrations are strongly coupled, i.e., delocalized over many bonds and atoms. Therefore the RR spectrum of TP cannot be described in terms of characteristic bands directly related to

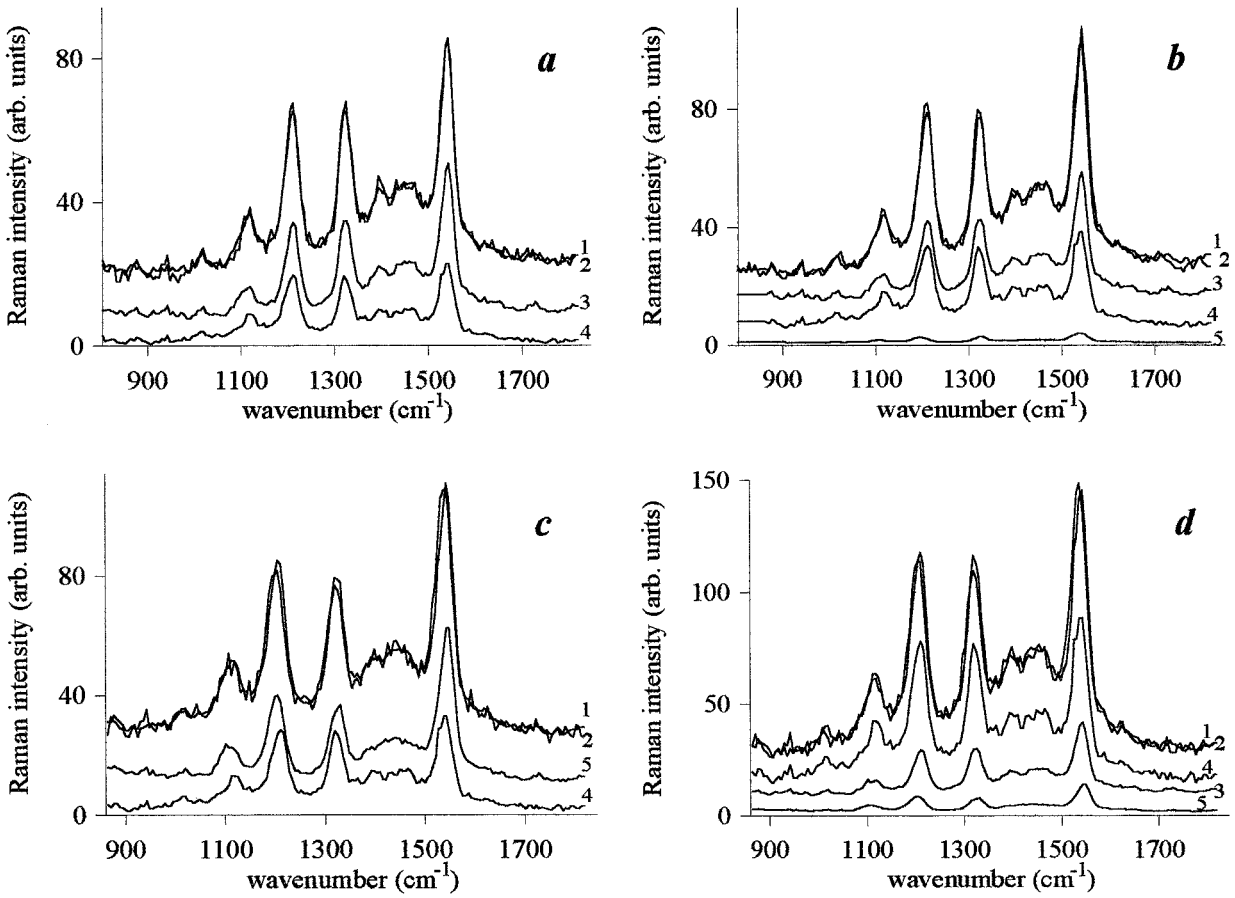

FIGURE 2 Several examples of the spectral analysis (the decomposition procedure) of RR spectra (*1*) recorded from within the nucleus (*a*), cytoplasm (*b*), and lysosomes (*c* and *d*) of TP-treated cells. The decomposition of measured spectra into components was performed using a set of reference spectra that describe TP bound to proteins (*3*), monomeric TP (*4*), and aggregated TP (*5*). The validity of the decomposition procedure can be estimated by comparing an extent of coincidence of spectrum 2 simulated on the basis of components 3–5 with the experimental spectrum 1. Spectra 3–5 show the relative contribution of each component to the overall spectrum.

vibrations of particular groups of atoms. But vibrational mode analysis provides an estimation of the relative involvement of N_α, N_β, C_α, and C_β atoms in different vibrations (Table 1), which may help to recognize molecular interactions of TP that occur with the participation of these atoms. It should be noted that the relative intensity of the RR bands of TP depends considerably on the polarization of the excitation light (data not shown). In the present study all of the RR measurements were performed with nonpolarized light from a He-Ne laser.

The TP was reported to be highly photostable in aqueous solution (Kaliya et al., 1999). Indeed, the RR spectrum measured with a rotated quartz cell from TP solution deoxygenated with nitrogen and that of one recorded with a stationary quartz cell from TP solution saturated with oxygen were found to be identical. No differences were observed in RR spectra before and after prolonged (1 h) illumination of TP solution (100 μl, 10 μM) with a high-power-density laser light (20 W/cm^2, 676 nm wavelength). The exceptional photostability of the chromophore has predetermined the observed stability of the intracellular TP signal in the course of microspectroscopic measurements.

Spectrophotometric analysis has shown that the absorption spectrum of TP underwent a ~1-nm red shift in the saturated solution of DNA. This shift appeared after 30 min of incubation of the mixture at 37°C, indicating a very weak interaction between the drug and DNA. The absorption spectrum of TP bound to DNA calculated as described in Materials and Methods has a 677-nm maximum. The extent of TP binding (α) to DNA was estimated to be ~6–8%. Very weak interaction of TP with RNA was detected with spectrophotometry only after 60 min of incubation of the mixture at 37°C. Calculated absorption spectrum of TP bound to RNA has a 696-nm maximum. The extent of TP binding (α) to RNA was ~4–6% under the experimental conditions used. No noticeable changes in the RR spectra of TP/DNA and TP/RNA mixtures as compared with that of TP were found.

TABLE 1 Frequencies (cm^{-1}), intensities, and assignments of vibrational modes of TP

Monomeric TP			TP bound to proteins			Aggregated TP				Involvement in vibration*†			
Freq.	I_{rel} (%)‡	$\sigma^{\|}$	Freq.	I_{rel} (%)‡	$\sigma^{\|}$	Freq.	I_{rel} (%)‡	Assignments*		N_α	N_β	C_α	C_β
1013	20	1.6	1013	6	1.4	1013 (0)§	3	ν_{23}	A_{2g}				
1117	40	3.3	1117	20	4.8	1110 (−7)	20	ν_{14}	B_{1g}	++	+	+	+++
1210	90	7.3	1210	60	14.4	1200 (−10)	50	ν_{13}	B_{1g}	++	++	++	++
1320	90	7.3	1320	65	15.6	1325 (+5)	40	ν_{12}	B_{1g}	+++	+	+++	++
1396	40	3.2	1396	30	7.2	1390 (−6)¶	20	ν_{20}	A_{2g}				
1442	20	1.6	1442	20	4.8	1430 (−12)¶	20	ν_{29}	B_{2g}				
1466	30	2.4	1466	25	6.0	1464 (−2)¶	20	ν_{28}	B_{2g}				
1538	100	7.9	1538	100	23.9	1544 (+6)	100	ν_3	A_{1g}	+	+	+++	++

*The assignments were taken from previous work (Bartholomew et al., 1989).
†Relative involvement in vibration of some phthalocyanine atoms (Fig. 1): large (+++), medium (++), small (+).
‡Relative intensity of RR bands in TP spectrum at λ_{exc} = 632.8 nm (nonpolarized light) normalized to the ν_3 band.
§Frequency shift as compared with the spectrum of monomeric free TP is given in parentheses.
¶Bands in the 1380–1480 cm^{-1} region are poorly resolved in the spectrum of aggregates.
‖Raman cross section of vibrational mode at the 632.8-nm excitation wavelength, in millibarns/(molecule steradian).

Spectrophotometric analysis has shown that TP was able to form complexes with amino acids and bovine serum albumin (BSA) (Kaliya et al., 1999). The ability of TP to bind to proteins was further studied with a model set of proteins including lysozyme, human serum albumin (HSA), and BSA. In addition, TP interaction with the pool of nonhistone nuclear proteins and histone H2A was investigated. It was found that TP binds tightly to nonhistone nuclear proteins, histone H2A, and lysozyme. TP formed complexes with HSA more readily than with BSA. Interactions between TP and the proteins were observed as a 12–15-nm red shift of the Q band in absorption spectra and noticeable changes in the RR spectrum of the drug (Table 1). The values of α determined with spectrophotometry were equal to 93%, 64%, 82%, 46%, and 86% in the cases of HSA, BSA, histone H2A, lysozyme, and the pool of nonhistone nuclear proteins, respectively. It is obvious that the TP ability to bind to proteins is considerably greater than its ability to form complexes with nucleic acids. Side chains of many amino acid residues can participate in TP binding. Spectrophotometric analysis shows that TP forms complexes with histidine, arginine, lysine, tryptophan, and, to a lesser degree, with phenylalanine, whereas no interactions were detected with tyrosine or negatively charged amino acids.

Changes in RR spectra of TP induced by interactions with any one of the studied proteins were very similar, namely, a moderate decrease in the relative intensities of the 1013, 1117, 1210, 1320 cm^{-1} bands as compared to that of the 1538 cm^{-1} band without any frequency shifts, and moderate enhancement of RR cross sections of vibrational modes (Table 1). It is obvious that TP interactions can occur via the carboxylic groups, via the nitrogen atoms, and/or via the cobalt atom. As was mentioned above, the carboxylic groups are weakly conjugated with the π-electron system of phthalocyanine. Therefore, although their participation in the interactions of TP with proteins may take place, it cannot noticeably disturb the RR spectrum of TP. Bands that undergo relative intensity changes contain a large contribution from vibrational movements of the nitrogen atoms (Table 1). Therefore it can be envisaged that interactions of the nitrogens and/or the cobalt with external ligands are responsible for alterations in the RR spectrum. Earlier it was shown (Gavrilov et al., 1980; Kaliya et al., 1999) that derivatives of cobalt (II) phthalocyanines (PcCo(II)) form axially coordinated complexes with ligands (L) $PcCo(II)L_n$, where n = 1, 2, and can be further oxidized to $[PcCo(III)L_n]^+$. It was concluded that formation of $[PcCo(III)L_2]^+$ was responsible for the changes in absorption spectra of TP associated with amino acids and proteins (Kaliya et al., 1999). Therefore, similar changes in RR spectra of TP bound to different proteins can occur because of the similar type of interactions leading to $[PcCo(III)L_2]^+$ formation.

TP is not soluble in pure methanol, ethanol, or nonpolar solvents. Absorption spectra of TP mixed with the micelles of sodium dodecyl sulfate (SDS) or Triton X-100 are not changed as compared to the spectrum of TP in aqueous solution. From examination of RR spectra, no interaction was detected between TP and detergent micelles, even at the vibrational level. Eight negative charges situated symmetrically around the phthalocyanine core screen the hydrophobic nucleus of the molecule and exclude not only penetration into the hydrophobic region of micelles but even TP binding at their polar surface.

It was found that the carboxylic groups make TP sensitive to pH and divalent metal cations (Kaliya et al., 1999). A decrease in pH from 6 to 5 induces protonation of the carboxylic groups, followed by aggregation and precipitation of TP. Ca^{2+} cations bind to carboxylic groups, leading to formation of an insoluble salt of TP and its precipitation. RR spectra of monomeric and aggregated drug differ considerably (Table 1). Upon aggregation the 1110, 1200, 1390, and 1430 cm^{-1} bands undergo remarkable down-

frequency shifts, whereas the 1325 and 1544 cm^{-1} bands are shifted to higher frequencies. The frequency shifts are accompanied by changes in relative intensities of the bands (Table 1) and a considerable decrease in integrated intensity of the RR signal. The RR spectrum of pH-induced aggregates, the spectrum of aggregates formed in the presence of divalent cations, and the spectrum of a polycrystalline powder of the sodium salt of TP are very similar. Therefore, the observed spectral features should be attributed to interchromophore interactions within aggregates.

Molecular interactions of TP in the presence of ascorbate

Molecular interactions of TP were studied in the presence of ascorbate with spectrophotometry and RR spectroscopy. Special attention was paid to the changes that could appear in RR spectra.

In the presence of ascorbate some molecules of TP undergo oxidation (Prof. S. A. Borisenko, personal communications). This is clearly observed as a time-dependent decrease in the absorbance of the solution at 675 nm. The integrated intensity of the RR signal decreases in the presence of ascorbate, but RR spectra of TP do not change. Oxidized TP does not absorb in the red region, and, therefore, it does not contribute to RR spectra. As a result, an increase in the number of oxidized molecules is observed just as a decrease in intensity of the RR spectrum.

It was found that both oxidation of TP and its action as catalyst were abolished by TP binding to HSA (Prof. S. A. Borisenko, personal communications). Our experiments show that absorption and RR spectra of the studied TP/protein complexes do not change when ascorbate is added, thus 1) confirming that oxidation of TP bound to proteins is reduced sharply and 2) indicating that interactions between TP and proteins are not affected by ascorbate. Binding of TP to the components of culture media and fetal calf serum is also accompanied by a considerable decrease in the drug oxidation by ascorbate. Analysis of absorption and RR spectra indicates that the presence of ascorbate does not enhance binding of TP to DNA or RNA.

RR spectra of TP inside living cells and their analysis

Microspectroscopic experiments show that TP penetrates into living A549 cells and accumulates within the cytoplasm and nucleus. Analysis of RR spectra recorded from within various cellular compartments indicates that, besides integrated intensity, spectra are different in relative intensity and position of bands. Using the procedure of spectral decomposition, we revealed that intracellular spectra can be presented as a linear combination of RR spectra of TP_{mono}, $TP_{bnd,}$ and TP_{agg} (Fig. 2). Cellular molecules do not contribute noticeably to the measured spectra because there are no cellular chromophores that are in resonance with the excitation used. Even the intrinsic cellular fluorescence, the main problem for Raman microspectroscopy in the visible region, is negligible at an excitation wavelength of 632.8 nm. Nonresonance Raman scattering of cellular molecules is several orders less intensive than the RR signal of TP. As a result, despite high local concentrations of cellular molecules, they provide only a weak nonresolved background contribution to the observed RR spectra.

After spectral decomposition was carried out it was clearly seen that the RR spectrum of TP within the nucleus is predominantly a superposition of signals of TP_{mono} and TP_{bnd} (Fig. 2 *a*). In addition to TP_{mono} and TP_{bnd} the contribution of TP_{agg} to the overall drug spectrum is observed distinctly within cytoplasmic compartments (Fig. 2 *b*). As is discussed below, the signal of TP_{agg} can dominate within lysosomes under certain conditions (Fig. 2 *c*). Careful examination of hundreds of spectral images measured from cells incubated with TP or TP/ascorbate mixture at various regimes of treatment enables one to conclude that intracellular RR spectra of the drug can be reliably described using the set of TP_{mono}, TP_{bnd}, and TP_{agg} model spectra. In other words, three different states of the drug, namely monomers, aggregates, and complexes with proteins, can be recognized and mapped within living cells with the CSI technique. It should be mentioned that monomeric TP can be free or bound to cellular molecules via carboxylic groups. The interactions occurring predominantly via carboxylic groups do not affect absorption and the RR spectrum of chromophore moiety, and therefore drug molecules bound this way cannot be distinguished from free TP.

Localization, uptake, and retention of TP within A549 cells

Analysis of spectral images (Figs. 3–5) clearly shows that TP is distributed throughout the cytoplasm and accumulates within the nucleus. The nucleus is uniformly stained with TP. In some cells the more intense accumulation of the drug within nucleoli than that within nucleoplasm is observed (Figs. 3 and 5). The cytoplasmic distribution of TP is rather diffuse after 10 min of cell incubation with the drug (Fig. 3 *I*). Besides uniform staining, small inclusions with highly concentrated drug are observed in cytoplasm at incubation times longer than 1 h (Figs. 3–5). Similar patterns of TP intracellular accumulation and distribution were observed in cells incubated with 400 or 100 μM of the drug.

To reveal the origin of these inclusions, cells incubated with TP were further treated with AO, the red fluorescence of which was a label for lysosomes. Comparing an epifluorescence image of the AO-marked lysosomes with a RR confocal spectral image of TP distribution, one can note that localization of the drug containing inclusions coincides precisely with that of lysosomes (Fig. 6). Some lysosomes

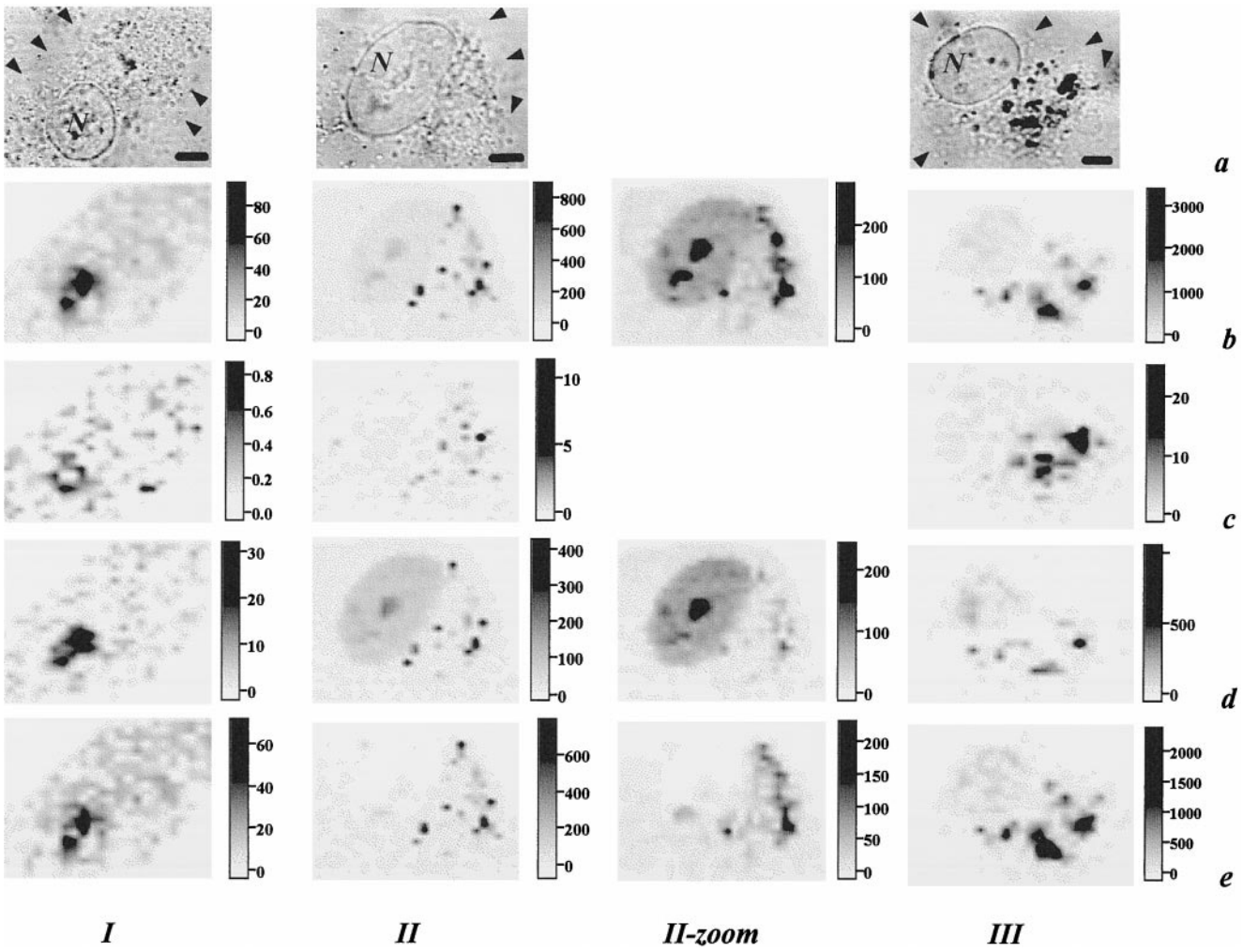

FIGURE 3 Confocal spectral images of cells exposed to 400 μM TP for 10 min (*I*), 1 h (*II*), and 14 h (*III*). (*a*) Conventional light-microscope image of the cell. (*b–e*) Spectral images describing the subcellular distribution of TP_{agg} (*c*), TP_{bnd} (*d*), and TP_{mono} (*e*), as well as total TP except for TP_{agg} (*b*). Low concentration patterns of subcellular distribution of TP are shown in column II-zoom. Scales show the concentration of TP in μM for the images *b*, *d*, and *e* as well as the relative intensity of signal in arbitrary units for image *c*. (*a*) Arrowheads indicate the boundary of the cell; *N* marks the nucleus; the bar represents 5 μm.

are not seen in the spectral image of TP. This can mean that TP is distributed among lysosomes heterogeneously. Besides, one has to keep in mind that all of the lysosomes are detected with the epifluorescence method, whereas the CSI technique measures the signal only from those lysosomes that are located within a thin optical section defined by the confocal conditions. Movement of lysosomes is another factor that hampers the registration of precisely coincident images of TP and lysosome distribution.

Diffused staining of cytoplasm with TP around the nucleus was found to not match the filamentous pattern of mitochondria distribution revealed with Rh123, a selective label for active mitochondria (data not shown). Therefore it may be deduced that there is no predominant accumulation of TP within mitochondria.

Penetration of TP into the A549 cell is rather fast despite the presence of eight negative charges per molecule. After 10 min of incubation the drug is already observed within the cytoplasm and the nucleus of the cell (Figs. 3 and 7). Its average intracellular concentration (AIC) reaches 8% of extracellular theraphthal concentration ($[TP]_{ext}$) (drug concentration saving aggregates is quantified). During 3 h of cell exposure to the drug AIC grows continuously up to 30% of $[TP]_{ext}$. Further intracellular accumulation of TP becomes much slower. When the incubation time rises from 3 h to 14 h the AIC increases from 30% to 43% of $[TP]_{ext}$ only (Fig. 7 *a*).

Distribution of TP as a whole and, singly, TP_{mono}, TP_{bnd}, and TP_{agg} among the cytoplasm and the nucleus was measured in the course of drug uptake and efflux (Figs. 3–5 and 7). Characteristic features of the kinetics of nuclear and cytoplasm accumulation of TP are very similar to those of AIC of the drug. At the same time the nuclear concentration of TP is ~1.5-fold higher than the cytoplasmic one during

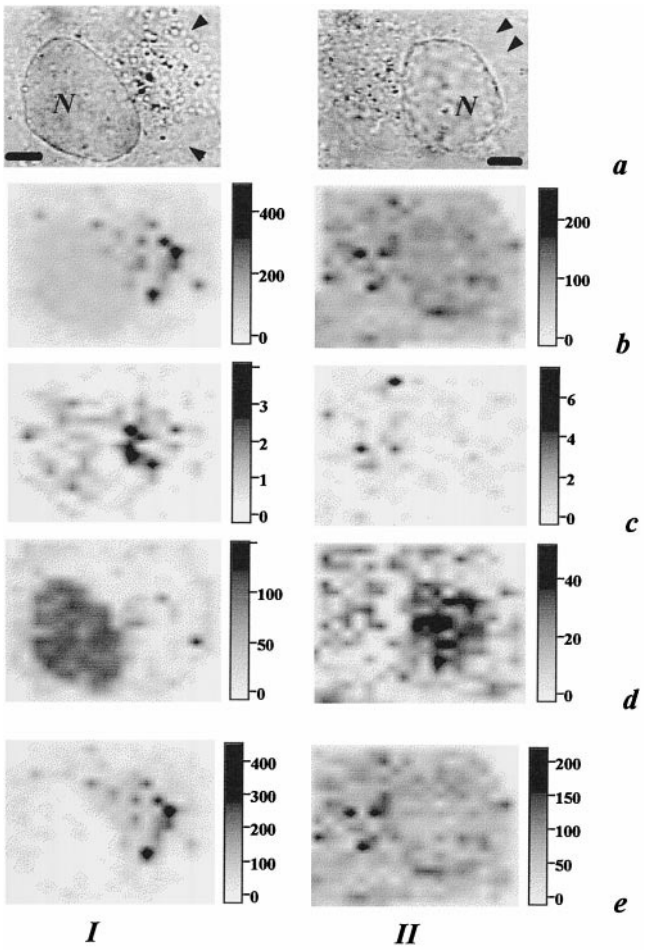

FIGURE 4 Confocal spectral images of cells exposed to 400 μM TP (*I)* and 400 μM/8 mM TP/ascorbate mixture *(II)* for 3 h. (*a*) Conventional light-microscope image of the cell. Spectral images describing the subcellular distribution of TP_{agg} (*c*), TP_{bnd} (*d*), and TP_{mono} (*e*), as well as total TP except for TP_{agg} (*b*). Scales show the concentration of TP in μM for the images *b*, *d*, and *e* and the relative signal intensity in arbitrary units for image *c*. (*a*) Arrowheads indicate the boundary of the cell; *N* marks the nucleus; the bar represents 5 μm.

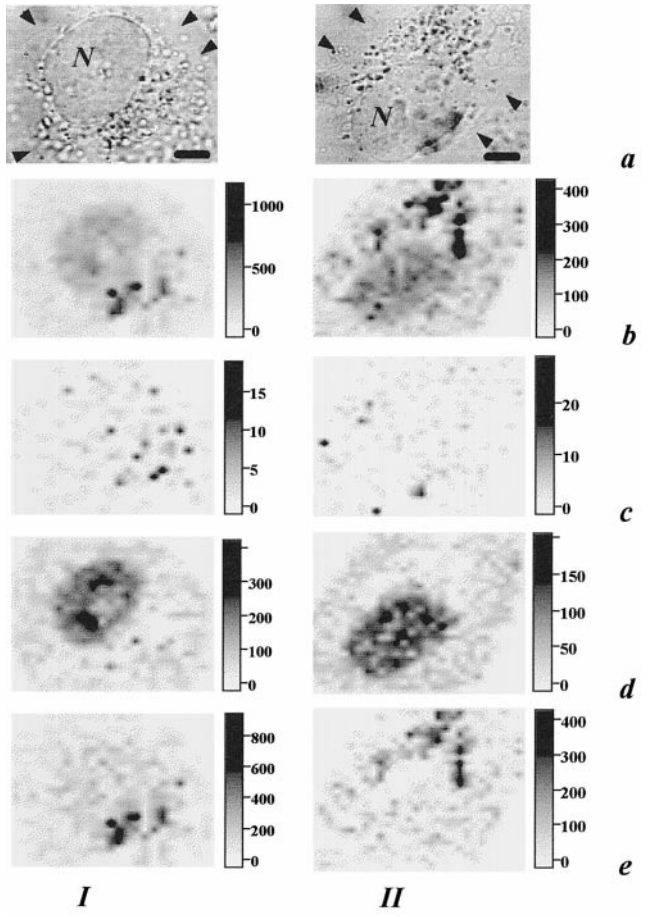

FIGURE 5 Confocal spectral images of cells exposed to 400 μM TP for 6 h, immediately after the exposure period (*I)* and after additional incubation in drug-free medium for 9 h *(II).* (*a*) Conventional light-microscope image of the cell. (*b*—*e*) Spectral images describing the subcellular distribution of TP_{agg} (*c*), TP_{bnd} (*d*), and TP_{mono} (*e*), as well as total TP except for TP_{agg} (*b*). Scales show the concentration of TP in μM for images *b*, *d*, and *e* as well as the relative intensity of signal in arbitrary units for image *c*. (*a*) Arrowheads indicate the boundary of the cell; *N* marks the nucleus; the bar represents 5 μm.

uptake (Fig. 7 *a*). Analysis shows that this difference is directly related to the nuclear concentration of TP_{bnd}, which is approximately threefold higher than the concentration of TP_{bnd} within cytoplasm (Fig. 7 *c*). TP_{mono} is distributed between nucleus and cytoplasm in a more equivalent manner (Fig. 7 *b*). Pronounced accumulation of the drug within lysosomes is observed in cells incubated with TP for 1 h and longer (Figs. 3–5). The intralysosome concentration of TP is five- to eightfold higher than the drug concentration in the surrounding cytoplasm. TP_{mono}, TP_{bnd}, and TP_{agg} are detected within lysosomes, but TP_{mono} dominates there. Aggregation of the drug in lysosomes is enhanced as the incubation time increases. The appearance of blue spots is observed with the light microscope in the cytoplasm of cells incubated with TP for 14 h (Fig. 3 *IIIa*). Spectral analysis shows a very high (up to 3 mM) concentration of TP and a considerable amount of TP_{agg} within the lysosomes of these cells (Fig. 3 *III*).

Efflux of TP in opposition to its uptake was found to be very slow. Cells incubated with the drug for 6 h and then grown in drug-free medium for 2 or 9 h still contained a considerable amount of the drug (Figs. 5 and 7). Analysis shows that AIC of TP is reduced just 1.3-fold during 9 h of efflux. Release of drug from the nucleus and cytoplasm occurs in a similar manner (Fig. 7). As a result, patterns of localization and relative intracellular distribution of TP_{mono} and TP_{bnd} are not changed during drug efflux (Fig. 5). A remarkable decrease in intranuclear content of TP_{agg} and its increase in the cytoplasm domain (mainly within lysosomes) are observed (Fig. 7 *d*).

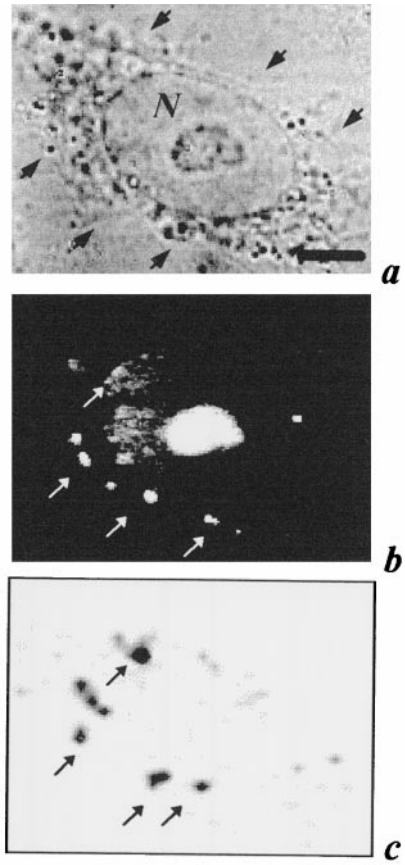

FIGURE 6 Confocal spectral images of the cell exposed to 400 μM TP for 1 h and stained after that with AO. (*a*) Conventional light-microscope image of the cell. (*b*) Epifluorescence image corresponding to red fluorescence of AO. (*c*) Spectral image of subcellular distribution of TP. (*a*) Arrowheads indicate the boundary of the cell; *N* marks the nucleus; the bar represents 6 μm. (*b* and *c*) Arrows indicate the lysosomes, where accumulation of TP is observed. (*c*) Black corresponds to the highest signal intensity.

Intracellular accumulation and action of TP/ascorbate catalytic system

Incubation of A549 cells with a TP/ascorbate mixture induces inhibition of cell proliferation (Fig. 8). The control experiment with ascorbate alone shows no noticeable cytotoxic action of sodium ascorbate. Incubation of cells with TP alone reveals moderate concentration-dependent cytotoxicity of the agent, which is considerably lower than the effect of the TP/ascorbate system.

To discover the critical intracellular targets of the cytotoxic action of the TP/ascorbate catalytic system, selective organelle labeling was carried out. Intact A-549 cells treated with AO show a rather homogeneous structure of the cytoplasmic matrix and ~10–100 red colored lysosomes located mostly in close vicinity to the nucleus. A549 cells have filamentous mitochondria radiating from the perinuclear region, as visualized with Rh123. EtBr used as a vitality test does not penetrate into living A549 cells. Incubation of cells with TP or ascorbate separately does not cause any changes in lysosome or mitochondria staining.

After 1 h of treatment with the TP/ascorbate mixture, one can see a noticeable decrease in the amount of lysosomes. The cytoplasmic matrix becomes rough and heterogeneous. The distribution and activity of the mitochondria stay unchanged. A few cells have numerous tiny blebs on the cell membrane and orange nuclei colored with EtBr, which indicates some disturbance of the plasma membrane permeability.

Incubation of cells with TP/ascorbate mixture for 3 h leads to disruption of lysosomes. Fragmentation of the filamentous network of mitochondria is observed; most of them adopt a globular shape. The CSI analysis shows that the distribution of TP within the nucleus and the cytoplasm becomes rather uniform (Fig. 4). Inclusions containing a high concentration of TP are not observed in these cells, thus confirming their assignment to lysosomes, which are destroyed under radical attack.

Further treatment of cells with the BCS results in inflation of cytoplasm, cell rounding, and cariopyknosis. Intense blebbing of external membrane and staining of the nucleus with EtBr now become the characteristics of many cells. Lurid staining of the cytoplasmic matrix and nucleus with AO can be considered to be due to the appearance of denatured forms of nucleic acids or a decrease in cytoplasmic pH due to the leakage of lysosome content into the cytoplasm.

Treatment of cells with TP/ascorbate mixture leads to a ~1.5-fold decrease in AIC of the drug as compared to cells incubated with TP alone. The decrease in TP concentration occurs equally within the cytoplasm and nucleus of cells for TP_{mono}, TP_{bnd}, and TP_{agg} (Fig. 7) and may be related to the destruction of TP itself during the catalysis of ascorbate autooxidation.

DISCUSSION

The RR CSI analysis revealed that TP is distributed throughout cytoplasm and is localized preferentially within the nucleus of A549 cells (Figs. 3–5 and 7). A diffused pattern of TP distribution within the nucleus is complemented by slightly more intense staining of nucleoli in some cells. Rather uniform staining of cytoplasm is accompanied by considerable accumulation of TP within lysosomes. Mitochondria do not accumulate TP. Model experiments in solution have shown that TP has a very low ability to bind to or to penetrate into membranous systems. Accordingly, staining of plasmalemma or nuclear membrane with TP is not observed. It can be concluded that TP is localized within hydrophilic cytoplasmic domains. Nuclear localization of TP is the main feature of the pattern of agent distribution in the A549 human adenocarcinoma cells as compared with that observed for TP in K562 human erythroleukemic cells (Arzhantsev et al., 1999). This feature is probably related to

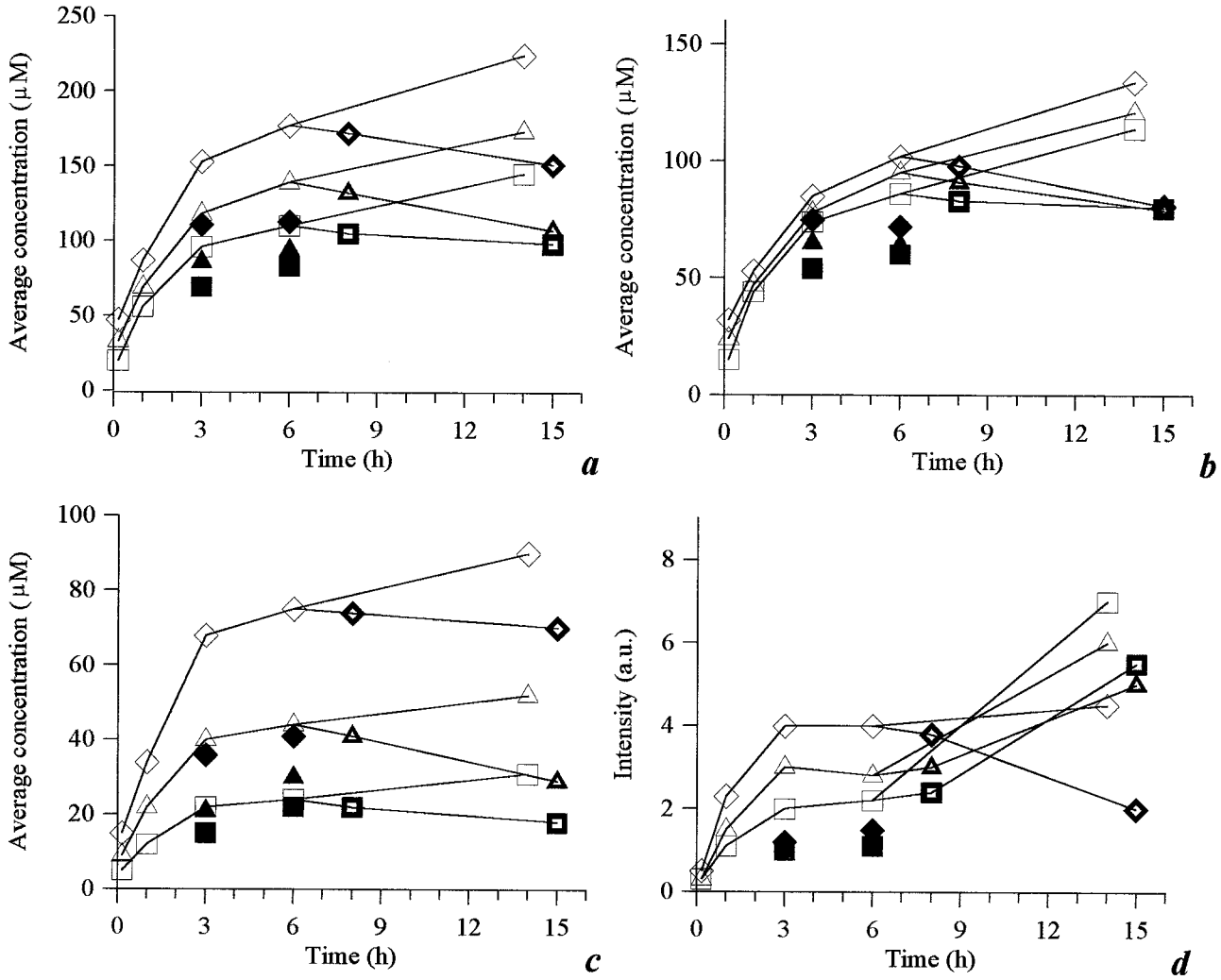

FIGURE 7 Average intracellular (*triangles*), intranuclear (*rhombuses*), and cytoplasmic (*squares*) concentrations of total TP, except for TP_{agg} (*a*), TP_{mono} (*b*), TP_{bnd} (*c*), and TP_{agg} (*d*) at different times of incubation of A549 cells with 400 μM TP (*open symbols*) and 400 μM/8 mM TP/ascorbate mixture (*closed symbols*). Retention of TP in the cells incubated with 400 μM TP for 6 h is shown by demiclosed symbols. Measurements of concentration have been performed with the RR CSI technique as described in Materials and Methods.

the origin of cells and requires further investigation, because distinctions in the intracellular localization of TP can be a reason for the different sensitivities of particular cancer cells to the action of BCS.

Three states of the drug were recognized and mapped within living cells with the CSI technique, namely TP_{mono}, TP_{bnd}, and TP_{agg}. The presence of TP bound to proteins and aggregated TP within living cells is in accordance with the properties of the drug observed during the study of molecular interactions of TP in solution. According to the model experiments, at least two factors can cause or assist drug aggregation, namely protonation of carboxyl groups at low pH and complexation with divalent cations.

Eight negative charges do not prevent TP from rapidly penetrating A549 cells. Fluid phase pinocytosis may be the main mechanism of uptake of hydrophilic TP. Endocytosis also seems to be important for the internalization of TP bound to proteins. Diffusional processes of transport of TP into and out of the cell are considered to be rather weak, mainly because of the large negative charge of the molecule. This is indirectly confirmed by very low efflux of the drug during the first period of cell incubation in drug-free medium. Intracellular accumulation of TP is relatively low compared to many other antitumor drugs. For example, intracellular concentration of mitoxantrone achieves a 50–80-fold excess over its extracellular concentration (Feofanov et al., 1997a).

Despite low intracellular accumulation the cytotoxic activity of the TP/ascorbate system (IC_{50} = 14 μM) is on the same order as that induced by some chemotherapy agents, particularly cisplatin (*cis*-dichlorodiammine platinum (II), IC_{50} = 26 μM). It may be concluded that because of

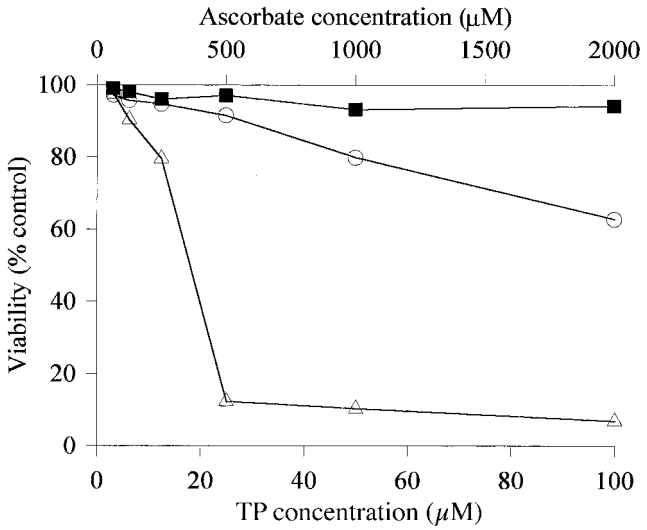

FIGURE 8 Concentration-response curves for survival of A549 cells after exposure to TP (*open circles*), ascorbate (*closed squares*), and TP/ascorbate mixture at molar ratio 1/20 (*open triangles*). The ordinate is the survival of tumor cells expressed as a percentage of control. Abscissa: The upper axis is the concentration of ascorbate (*closed symbols*); the lower axis is the concentration of TP (*open symbols*). For details see Materials and Methods.

peculiarities of intracellular distribution of TP the TP/ascorbate system is efficient at inducing numerous types of damage to subcellular organelles and cellular molecules. Lysosome damage followed by the leakage of its contents into the cytoplasm has been documented as one of the primary events in the course of BCS action. This allows these organelles to be considered one of the initial targets of the BCS action. Disruption of mitochondrial structure was detected, although mitochondria were not identified as a major subcellular site of TP localization. This effect is probably mediated by a radical attack from the cytosol and/or is related to the leakage of lysosomal enzymes into the cytoplasm, but it is not induced by site-directed action of the BCS. Plasma membrane injury should be considered a secondary effect of the BCS action, appearing only several hours after activation of the BCS. It is in accordance with a low affinity of the TP/ascorbate system for membranous structures.

Preferential nuclear accumulation of TP is probably responsible for the induction of nuclear component damage. The drug is partially bound to nuclear proteins. Both nonhistone proteins and histones form complexes with TP. Formation of complexes between TP and histones seems to be facilitated by electrostatic interaction of negatively charged carboxylic groups of the drug with multiple positively charged amino acid side chains of the proteins. Binding sites of many nonhistone nuclear proteins have optimal structures for interaction with negatively charged nucleic acids, so TP is most probably bound within these sites. Histones are part of the nucleosome complexes. So, more exactly, within nucleosomes TP has to be bound to histones. Although the tendency toward direct interaction between TP and DNA is very slight, a high concentration and a close proximity of the radical-generating system to DNA are obvious. Radical-induced cleavage of DNA and oxidation of nucleotide bases can proceed. The occurrence of these processes in the case of the TP/ascorbate system was observed in vitro (Belkov et al., 1996). It has to be mentioned that in the case of nonhistone proteins the reduced catalytic activity of TP bound to proteins may be overcompensated by direct oxidation of functionally important amino acid residues within the sites of nucleic acid binding, where TP also seems to be bound.

It has to be mentioned that the observed weak cytotoxicity of TP itself (Fig. 8) can also be related to the drug's ability to bind to nonhistone proteins. Competing to some extent with the nucleic acids for binding to proteins of gene machinery, TP can inhibit some of the processes of gene regulation, transcription, etc. To clarify the types of DNA and nuclear protein damage and their relative roles in the overall cytotoxic effect of the TP/ascorbate system, extensive additional investigations are required. Some of these experiments are currently under way.

The BCS based on the TP/ascorbate mixture is very promising for antitumor therapy, and it is currently at phase I of clinical trials. Several other BCSs that were proposed recently indicate that a binary catalytic therapy for malignant tumors will be further developed. Therefore, the RR CSI technique will be required as a unique tool applicable to the detection of nonfluorescent transition metal complexes within living cells. The present work is among the first to reveal the potential of the method in this field. It demonstrates the uses for the RR CSI technique, namely 1) revealing intracellular localization and quantitative distribution of the catalyst among particular cellular compartments; 2) identification of organelles selectively accumulating the drug as potential critical targets of its action; 3) quantitative study of kinetics of the catalyst uptake and efflux; 4) study of intracellular state and molecular interactions of the drug in relation to the drug activity.

As compared to the wide-field Raman imaging methods, the RR CSI technique provides two important features: the confocal mode of measurement and recording of the whole spectrum at each point in the cell. The confocal regime allows resolution and sharpness of details to be improved in Raman images through the suppression of signals from specimen layers above and below the scanning optical section. But, what is more important, it is a basis for quantitative measurements. The thickness of the scanning layer is fixed during all of the measurements, and it is less than the thickness of the cell. So the intensity of a spectrum is proportional to the intracellular concentration of the drug. By using a calibration procedure described in Materials and Methods, researchers can perform quantitative analysis.

Spectral analysis allows different states and molecular interactions of the drug to be reliably identified and mapped within living cells. This advantage of the RR CSI technique can be well illustrated, using TP as an example. It is not possible to indicate particular well-resolved Raman bands corresponding to TP_{mono}, TP_{bnd}, or TP_{agg} only and to use them for image measurement with the filtering Raman imaging methods. The whole spectrum should be analyzed with the spectral decomposition procedure to characterize the state of the drug at each point in a cell.

Beside living cells it is quite important to understand the peculiarities of accumulation and localization of catalytic component of BCSs within malignant tissues. To do this the RR CSI approach can be applied to analyze cryogenic tissue sections and biopsy probes from patients. Thus the RR CSI study of distribution and interaction of TP within tissue structures is in progress now.

We are indebted to L. G. Nikolaev for a gift of extract of nonhistone nuclear proteins and fruitful discussions. We thank Dr. V. L. Karpov for a gift of histone H2A. We are grateful to Prof. O. L. Kaliya and E. A. Lukyanets for a gift of theraphthal sample and useful discussions.

This research was supported by a grant from Moscow anticancer program. AIG was supported by the FEBS Summer Fellowship. AVF was supported by the FEBS Short Term Fellowship.

REFERENCES

Arzhantsev, S. Y., A. Y. Chikishev, N. I. Koroteev, J. Greve, C. Otto, and N. M. Sijtsema. 1999. Localization study of Co-phthalocyanines in cells by Raman micro(spectro)scopy. *J. Raman Spectrosc.* 30:205–208.

Bartholomew, C. R., A. A. McConnel, and W. E. Smith. 1989. Resonance Raman excitation profile of cobalt phthalocyanine at room temperature and 10 K. *J. Raman Spectrosc.* 20:595–600.

Carmichael, J., W. G. DeGraff, A. F. Gazdar, J. D. Minna, and J. B. Mitchell. 1987. Evaluation of a tetrazolium-based semiautomated colorimetric assay: assessment of chemosensitivity testing. *Cancer Res.* 47:936–942.

Belkov, V. M., N. F. Krynetskaya, Z. A. Shabarova, G. N. Novodarova, and M. E. Vol'pin. 1996. Transition-metal complexes as catalysts of active oxygen species formation in autooxidation reactions. 2. Oxidative degradation of nucleic acids by cobalt and iron phthalocyanine complexes. *Russ. Chem. Bull.* 45:2105–2111.

Bubnovskaya, L. N., M. E. Vol'pin, I. I. Ganusevich, I. Ya. Levitin, V. K. Onanezov, S. P. Osinsky, A. A. Pankratov, A. L. Sigan, V. V. Surgai, M. V. Tsikalova, and R. I. Iakubovskaya. 1998. Shiff-based Co-complexes as potent antitumor agents and anticancer therapy modifiers. *Mendeleev Chem. J.* 42:128–140.

Cameron, E., L. Pauling, and B. Leibovitz. Ascorbic acid and cancer: a review. 1979. *Cancer Res.* 39:663–681.

Clark, R. J. H., and R. E. Hester. 1993. Advances in Spectroscopy, Vol. 20, Biomolecular Spectroscopy, Part A. Wiley, Chichester, England.

Dignam, J. D., R. M. Lebovitz, and R. G. Roeder. 1983. Accurate transcription initiation by RNA polymerase II in a soluble extract from isolated mammalian nuclei. *Nucleic Acid Res.* 11:1475–1489.

Favard, C., P. Valisa, M. Egret-Charlier, S. Sharonov, C. Herben, M. Manfait, E. Da Silva, and P. Vigny. 1999. A new UV-visible confocal laser scanning microspectrofluorometer designed for spectral cellular imaging. *Biospectroscopy.* 5:101–115.

Feofanov, A., S. Charonov, F. Fleury, I. Kudelina, and I. Nabiev. 1997a. Quantitative confocal spectral imaging analysis of mitoxantrone within living K562 cells: intracellular accumulation and distribution of monomers, aggregates, naphtoquinoxaline metabolite and drug-target complexes. *Biophys. J.* 73:3328–3336.

Feofanov, A., S. Charonov, I. Kudelina, F. Fleury, and I. Nabiev. 1997b. Localization and molecular interactions of mitoxantrone within living K562 cells as probed by confocal spectral imaging analysis. *Biophys. J.* 73:3317–3327.

Feofanov, A., S. Sharonov, P. Valisa, E. Da Silva, I. Nabiev, and M. Manfait. 1995. A new confocal stigmatic spectrometer for micro-Raman and microfluorescence spectral imaging analysis: design and applications. *Rev. Sci. Instrum.* 66:3146–3158.

Fodor, S. P. A., R. A. Copeland, C. A. Grygon, and T. G. Spiro. 1989. Deep-ultraviolet Raman excitation profiles and vibronic scattering mechanisms of phenylalanine, tyrosine, and tryptophan. *J. Am. Chem. Soc.* 111:5509–5518.

Gavrilov, V. I., L. G. Tomilova, E. V. Chernih, O. L. Kaliya, I. V. Shelepin, and E. A. Lukyanets. 1980. Charge migration in products of single electron oxidation of cobalt phthalocyanine. *Zh. Obshch. Khim. (Russ.).* 50:2143–2144.

Greve, J., and G. J. Puppels. 1993. Advances in Spectroscopy, Vol. 20, Biomolecular Spectroscopy, Part A. R. J. H. Clark and R. E. Hester, editors. Wiley, Chichester, England. 231–265.

Halliwell, B., and C. H. Foyer. 1976. Ascorbic acid, metal ions and the superoxide radical. *Biochem. J.* 155:697–700.

Honegger, C. G., J. Torhorst, H. Langemann, A. Kabiersch, and W. Krenger. 1988. Quantitative determination of water-soluble scavengers in neoplastic and non-neoplastic human breast tissue. *Int. J. Cancer.* 15:690–694.

Kaliya, O. L., N. V. Teplyakova, Eu. A. Lukyanets, and G. N. Vorozhtsov. 1999. Study of physical-chemical properties and molecular interactions of cobalt (II) octa-4,5-carboxyphthalocyanine. *J. Porphyrins Phthalocyanines.* (in press).

Kimoto, E., H. Tanaka, J. Gyotoku, F. Morishige, and L. Pauling. 1983. Enhancement of antitumor activity of ascorbate against Ehrlich ascites tumor cells by the copper:glycylglycylhistidine complex. *Cancer Res.* 43:824–828.

Liu, K., L. Chen, R. Sheng, and M. D. Morris. 1991. Multispectral Hadamard-transform Raman microscopy. *Appl. Spectrosc.* 45: 1717–1720.

Pierson, H. F., J. M. Fisher, and M. Rabinovitz. 1985. Depletion of extracellular cysteine with hydroxocobalamin and ascorbate in experimental murine cancer chemotherapy. *Cancer Res.* 45:4727–4731.

Poydock, M. E. 1991. Effect of combined ascorbic acid and B-12 on survival of mice with implanted Ehrlich carcinoma and L1210-leukemia. *Am. J. Clin. Nutr.* 54:1261–1265.

Puppels, G. J., and J. Greve. 1996. Advances in Spectroscopy, Vol. 25, Biomedical Applications of Spectroscopy. R. J. H. Clark and R. E. Hester, editors. Wiley, Chichester, England. 1–47.

Puppels, G. J., M. Grond, and J. Greve. 1993. Direct imaging Raman microscopy based on tunable wavelength excitation and narrow band emission detection. *Appl. Spectrosc.* 47:1256–1267.

Sharonov, S., I. Chourpa, H. Morjani, I. Nabiev, M. Manfait, and A. Feofanov. 1994a. Confocal spectral imaging analysis in studies of the spatial distribution of antitumor drugs within living cancer cells. *Anal. Chim. Acta.* 290:40–47.

Sharonov, S., I. Nabiev, I. Chourpa, A. Feofanov, P. Valisa, and M. Manfait. 1994b. Confocal three-dimensional scanning laser Raman-SERS-fluorescence microprobe. Spectral imaging and high resolution applications. *J. Raman Spectrosc.* 25:699–707.

Sijtsema, N. M., S. D. Wouters, C. J. de Grauw, C. Otto, and J. Greve. 1998. Confocal direct imaging Raman microscope: design and applications in biology. *Appl. Spectrosc.* 52:348–355.

Syrkin, A. B., O. S. Zhukova, B. S. Kikot, L. G. Gatinskaya, E. M. Treshalina, R. I. Yakubovskaya, A. A. Pankratov, L. M. Mikhaylova, N. I. Zimakova, E. Yu. Kolesnikova, N. A. Oborotova, A. P. Polozkova, G. K. Gerasimova, O. L. Kaliya, S. G. Kuz'min, E. A. Luk'yanets, G. N. Vorozhtsov, and N. N. Trapeznikov. 1998. Theraphthal—new agent for binary catalytic therapy of malignant tumors. *Mendeleev Chem. J.* 42.5: 140–146.

Treado, P. J., I. W. Levin, and E. N. Lewis. 1992. Near-infrared acoustooptic filtered spectroscopic microscopy—a solid state approach to chemical imaging. *Appl. Spectrosc.* 46:553–559.

Treado, P. J., and M. D. Morris. 1990. Multichannel Hadamard-transform Raman microscopy. *Appl. Spectrosc.* 44:1–4.

Vol'pin, M. E., N. Yu. Krainova, I. Ya. Levitin, Z. Ya. Mitiaeva, G. N. Novodarova, V. K. Onanezov, A. A. Pankratov, V. I. Chissov, and R. I. Yakubovskaya. 1998. B_{12} compounds in combination with ascorbic acid as potential antitumor agents. *Mendeleev Chem. J.* 42.5:116–127.

Vol'pin, M. E., N. Yu. Krainova, I. V. Moskaleva, G. N. Novodarova, G. N. Vorozhtsov, M. G. Gal'pern, O. L. Kaliya, E. A. Luk'yanets, and S. A. Mikhalenko. 1996. Transition-metal complexes as catalysts of active oxygen species formation in autooxidation reactions. 1. Cobalt and iron phthalocyanine complexes. *Russ. Chem. Bull.* 45.8:2105–2111.

Vol'pin, M. E., G. N. Vorozhtsov, G. K. Gerasimova, O. S. Zhukova, N. I. Kazachkina, O. L. Kaliya, N. Yu. Krainova, I. Ya. Levitin, Yu. M. Luzhkov, E. A. Luk'yanets, G. N. Novodarova, E. M. Treshalina, A. B. Syrkin, V. I. Chissov, and R. I. Yakubovskaya. 1995. Agent for suppressing tumor growth. Patent PCT Int. Appl. WO 97 03,666. (Cl. A61K31/40), 6 Feb. 1997. RU, Appl. 95,112,240, 17 Jul; 16 pp. (Russ).

Williams, K. P. J., G. D. Pitt, B. J. E. Smith, A. Whitley, D. N. Batchelder, and I. P. Hayward. 1994. Use of a rapid-scanning stigmatic Raman imaging spectrograph in the industrial environment. *J. Raman Spectrosc.* 25:131–138.